Research Article

Hao Wang*, Yaliang Gui, Chaobo Dong, Salem Altaleb, Behrouz Movahhed Nouri, Martin Thomaschewski, Hamed Dalir* and Volker J. Sorger*

Self-powered broadband photodetector based on MoS_2/Sb_2Te_3 heterojunctions: a promising approach for highly sensitive detection

https://doi.org/10.1515/nanoph-2022-0413
Received August 10, 2022; accepted October 16, 2022; published online October 28, 2022

Abstract: Topological insulators have shown great potential for future optoelectronic technology due to their extraordinary optical and electrical properties. Photodetectors, as one of the most widely used optoelectronic devices, are crucial for sensing, imaging, communication, and optical computing systems to convert optical signals to electrical signals. Here we experimentally show a novel combination of topological insulators (TIs) and transition metal chalcogenides (TMDs) based self-powered photodetectors with ultra-low dark current and high sensitivity. The photodetector formed by a MoS_2/Sb_2Te_3 heterogeneous junction exhibits a low dark current of 2.4 pA at zero bias and 1.2 nA at 1V. It shows a high photoresponsivity of >150 mA W^{-1} at zero bias and rectification of 3 times at an externally applied bias voltage of 1V. The excellent performance of the proposed photodetector with its innovative material combination of TMDs and TIs paves the way for the development of novel high-performance optoelectronic devices. The TIs/TMDs transfer used to form the heterojunction is simple to incorporate into on-chip waveguide systems, enabling future applications on highly integrated photonic circuits.

Keywords: 2D material; broadband; photodetector; self-powered.

1 Introduction

Transition metal chalcogenides (TMDs) have been widely explored as active materials for high-performance optoelectronics due to their unique physical properties [1–3]. Transition metal chalcogenides optoelectronics usually suffers from surface oxidation, high contact resistance, and relatively low mobilities. To alleviate the aforementioned disadvantages of TMD-based photodetectors, recent technologies utilize plasmonic enhancement to improve the light–matter interaction of TMDs, while others use heterostructures to adjust inherent electrical and optical characteristics and graphene contact to aid charge carrier injection and extraction; those all exhibit attractive performance improvements such as higher sensitivity, broader frequency response, improved external quantum efficiencies (EQE), higher detectivity (D^*), and a broader spectral photoresponse [4–8]. However, combining topological insulators (TIs) as a novel quantum materials group with the attractive features of TMDs has remained largely unexplored. Topological insulators themselves exhibit various appealing optoelectronic features [9–11], which find applications in high-performance photodetection, e.g., due to their unique energy band structure. Furthermore, the topologically protected gapless conductive edge states or surface states in TIs offer extraordinarily high mobility and a broad detection spectrum compared to graphene, which has zero bandgaps [12–16]. Topological insulators are also mechanically flexible materials that can be used in wearable technology. Most TMDs are easily oxidized under atmospheric environments, whereas TIs are more stable in normal conditions. As a monolayer,

***Corresponding authors: Hao Wang**, Department of Electrical & Computer Engineering, The George Washington University, 800 22nd Street NW 5000 Science & Engineering Hall, Washington, DC 20052, USA; and Optelligence LLC, 10703 Marlboro Pike, Upper Marlboro, MD 20772, USA, E-mail: wang@optelligence.co. https://orcid.org/0000-0002-0444-6750; **Hamed Dalir**, Optelligence LLC, 10703 Marlboro Pike, Upper Marlboro, MD 20772, USA, E-mail: hamed.dalir@gmail.com. https://orcid.org/0000-0002-9998-3830; and **Volker J. Sorger**, Department of Electrical & Computer Engineering, The George Washington University, 800 22nd Street NW 5000 Science & Engineering Hall, Washington, DC 20052, USA, E-mail: sorger@gwu.edu. https://orcid.org/0000-0002-5152-4766
Yaliang Gui, **Chaobo Dong**, **Salem Altaleb**, **Behrouz Movahhed Nouri and Martin Thomaschewski**, Department of Electrical & Computer Engineering, The George Washington University, 800 22nd Street NW 5000 Science & Engineering Hall, Washington, DC 20052, USA. https://orcid.org/0000-0002-6085-3334 (Y. Gui)

molybdenum disulfide (MoS_2) has a direct bandgap of 1.8 eV, whereas, in bulk, it has an indirect bandgap of 1.3 eV [17]. The visible to the infrared absorption spectrum of MoS_2 ranges from 350 to 950 nm, which is utilized in various optoelectronic applications such as light harvesting, photovoltaics, and photodetection [18–23]. Heterojunctions are widely applied to self-powered photodetectors since the built-in electric field can efficiently separate the electron-hole pairs to enhance the photoresponsivity and speed under zero bias voltage. Different combinations of materials or technics have been demonstrated to improve the performance of the optoelectronic devices [24–28]. Recently, a tellurium at selenium roll-to-roll nanotube heterojunction and cadmium sulfide at cadmium selenide core/shell quantum dots showed the enhanced capacity for self-powered broadband photodetection but also significantly improved photocurrent density and stability in different environments [29, 30]. Here, we demonstrate a vertical heterojunction-based photodetector with TIs and TMDs, which provide a promising tool to bring different electrical and optical properties by creating the junction compared to the individual materials. The heterojunction-based photodetector, formed by MoS_2 and Sb_2Te_3 exfoliation and deterministic transfer to a silicon oxide substrate, shows reduced dark current, high responsivity $R = I_{photo}/P_{laser}$ (defined by the ratio between the photocurrent I_{photo} and the incident laser power P_{laser}), and a self-driven detection range from visible to near-infrared wavelengths. The photocarrier separation is accelerated, and photocarrier recombination is suppressed due to the inherent difference in their energy level. Compared to single TMDs, it also exhibits a reduced dark current, which is beneficial for achieving high detection sensitivities at reduced power consumption. The dark current is ~10 pA, and the light-induced on/off ratio is more than 10^3 due to the interlayer built-in field and a broadband response from 500 to 900 nm. Besides the demonstrated free-space application, the proposed device has potential in densely integrated applications such as digital to analog converter systems or photonic integrated circuits due to the ease of integration with photonic waveguide technology [31–33].

2 Results and discussion

To fabricate the device, Sb_2Te_3 and MoS_2 layers were prepared by mechanical exfoliation and transferred to a SiO_2/Si substrate by the pick and drop technique. These two layers are stacked by weak van der Waals force (Figure 1a). Three Ti/Au electrodes formed by electron beam evaporation act as the electrical contact pads to inject and extract the photocurrent generated by the photodetector. Two electrodes are placed on the top of the MoS_2, and one electrode is placed on the Sb_2Te_3 (Figure 1b). The compact total junction size is measured to be only 160 μm^2. A Schottky barrier is present when the electrode is contacted with the MoS_2/Sb_2Te_3 layers to reach the equilibrium state, and it also generates a tunneling current. The Schottky barrier height is strongly dependent on the metal work function. However, the applied heterostructure minimizes the depletion region due to the atomically thin layer. The photocarriers can be efficiently separated at the heterostructure interface with the built-in electric field in the PN heterojunction or an external electric field from an applied bias, yielding photocurrent across the heterostructure channel. As a result, there is no significant potential barrier in the forward direction, which increases the photodetector's responsivity (Figure 2a).

Raman and energy-dispersive X-ray spectroscopy (EDS) measurements are used to characterize the spatial structure and properties of the vertically stacked MoS_2/Sb_2Te_3 system. Raman spectra are collected via 532 nm laser illumination. The Raman signal of MoS_2 showed two distinct peaks at 384 cm^{-1} and 409 cm^{-1} in the spectrum Figure 2d, which indicated the in-plane Mo-S phonon mode (E^1_{2g} at 384 cm^{-1}) and out-of-plane Mo-S phonon mode (A_{1g} at 409 cm^{-1}) of MoS_2, respectively [34, 35]. Raman Spectra evidence the MoS_2 multilayer film with a stoke shift of 25 cm^{-1} [36]. The Raman spectrum of Sb_2Te_3 consists of different peaks related to Sb_2Te_3 vibrations: 70 cm^{-1}, 114 cm^{-1}, and 130 cm^{-1} with two minor peaks centered at 97 cm^{-1}, and 105 cm^{-1} between, and 146 cm^{-1}, 167 cm^{-1}. The 70 cm^{-1}, 97 cm^{-1}, and 167 cm^{-1} peaks indicated the A_{1g} and E_g normal modes of the Sb–Te vibrations. The 114 cm^{-1}, 105 cm^{-1}, and 146 cm^{-1} indicate the Te–Te interactions, which together consist of the whole structure of Sb_2Te_3 [36]. The thickness of Sb_2Te_3 is estimated to be above 65 nm [37]. Energy dispersive spectroscopy (EDS) is employed to explore the element information collected from the single layers (the exfoliated MoS_2 (point C), and Sb_2Te_3 (point A) and stacked layers (MoS_2/Sb_2Te_3 [point B]) on the device, respectively (Figure 2b). The corresponding MoS_2 EDS spectrum shows the *L* series peaks of Mo and S K_α peak is very pronounced; therefore, only a widened peak with a tail towards the high energy end can be seen with EDS. The elemental compositions (Sb/Te) of the exfoliated Sb_2Te_3 layers were also determined by EDS. We observed two weak X-ray emission peaks corresponding to Sb and Te. The spectrum

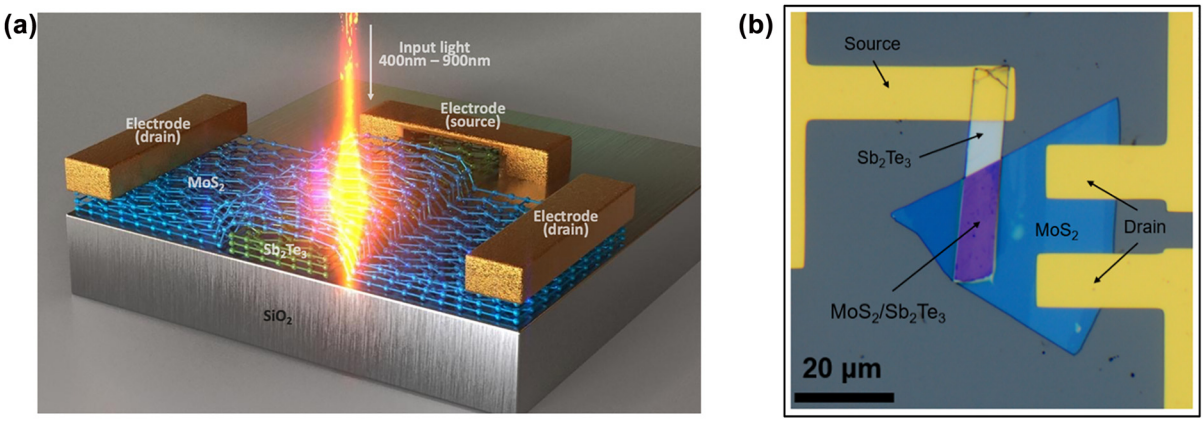

Figure 1: Sb_2Te_3/MoS_2 pn junction heterostructure photodetector. (a) A schematic representation of the Sb_2Te_3/MoS_2 van der Waals p-n junction photodetector. (b) The optical microscope image of PN junction device.

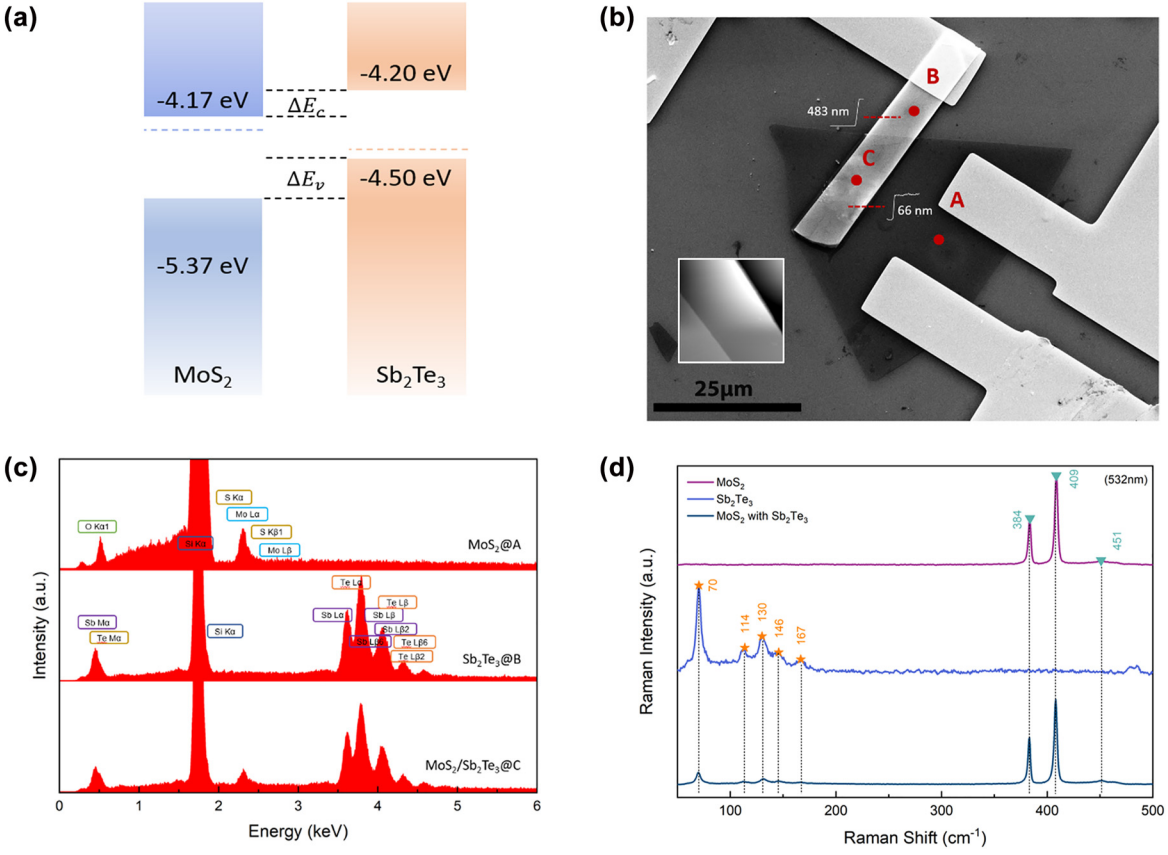

Figure 2: Material characterization of the Sb2Te3/MoS2 heterojunction. (a) Band structures of the vdW layered MoS_2/Sb_2Te_3 heterojunction (b) SEM image of the fabricated device with point A on Sb_2Te_3, point B on MoS_2 and point C on the MoS_2/Sb_2Te_3 heterojunction. Two electrodes are on top of the MoS_2 layer and one on top of the Sb_2Te_3. (c) As shown in the SEM image, EDS signals were collected at three distinct positions to characterize the materials. (d) Raman spectra were collected from the pure MoS_2 and $Sb2Te_3$ and the Sb2Te3/MoS2 PN junction region with a 532 nm laser.

also showed the characteristic peaks of Si, which originates from the used substrate. The absence of any other peaks indicates that the Sb_2Te_3 layers are formed from Sb and Te, only. The quantitative atomic ratio of Sb and Te is roughly 38.7–61.3%, which is near to the 2:3 stoichiometry ratio in accordance with the EDS investigations of Sb_2Te_3 [38–40].

Prior to the optoelectronic measurements, we characteristic the electrical performance of the MoS_2/Sb_2Te_3 junction by applying a source-drain bias voltage V_{sd} from −1 to 1 V to evaluate the dark current and performance of the van der Waals PN heterojunction. As indicated by the black curve in the I-V measurement (inset of Figure 3a–c), the dark currents are stable and consistent. The dark current is as low as 2.38 pA at zero bias and 1.16 nA at 1 V bias, which benefits from the heterostructure design. To our best knowledge, this is the lowest dark current in a vdW heterojunction photodetector compared to other vdW heterojunction photodetectors [41–49]. At a negative bias, the dark current becomes significantly higher than at positive voltages. Furthermore, under on and off bias voltage V_{sd}, the source-drain current, I_{sd} has a rectifying characteristic. This reveals that a vdW PN heterojunction is created at the interface of the stacked MoS_2/Sb_2Te_3, since the rectifying effect is observed under different bias voltages. The diode's on/off ratio, defined as the ratio between photogenerated current and dark current, is around 5.6×10^3. At room temperature, the ultra-low dark current and high on/off ratio at zero bias enable the development of a highly sensitive self-powered photodetector. The power-dependent IV measurement of the PN heterojunction at the wavelength of 500 nm, 700 nm, and 900 nm has also been performed (inset of Figure 3a–c). At zero bias voltage, the heterojunction separates the photogenerated electro-hole pairs and introduces the photocurrent due to the built-in electric field formed at the MoS_2/Sb_2Te_3 interface. The photocurrent I_{photo} increases with higher optical power illumination because electro-hole pairs generation rates increase. This demonstrates self-powered photodetection at various wavelengths (Figure 3a–c) with the insets in Figure 3a–c showing the measured I_{photo} and I_{sc} as a

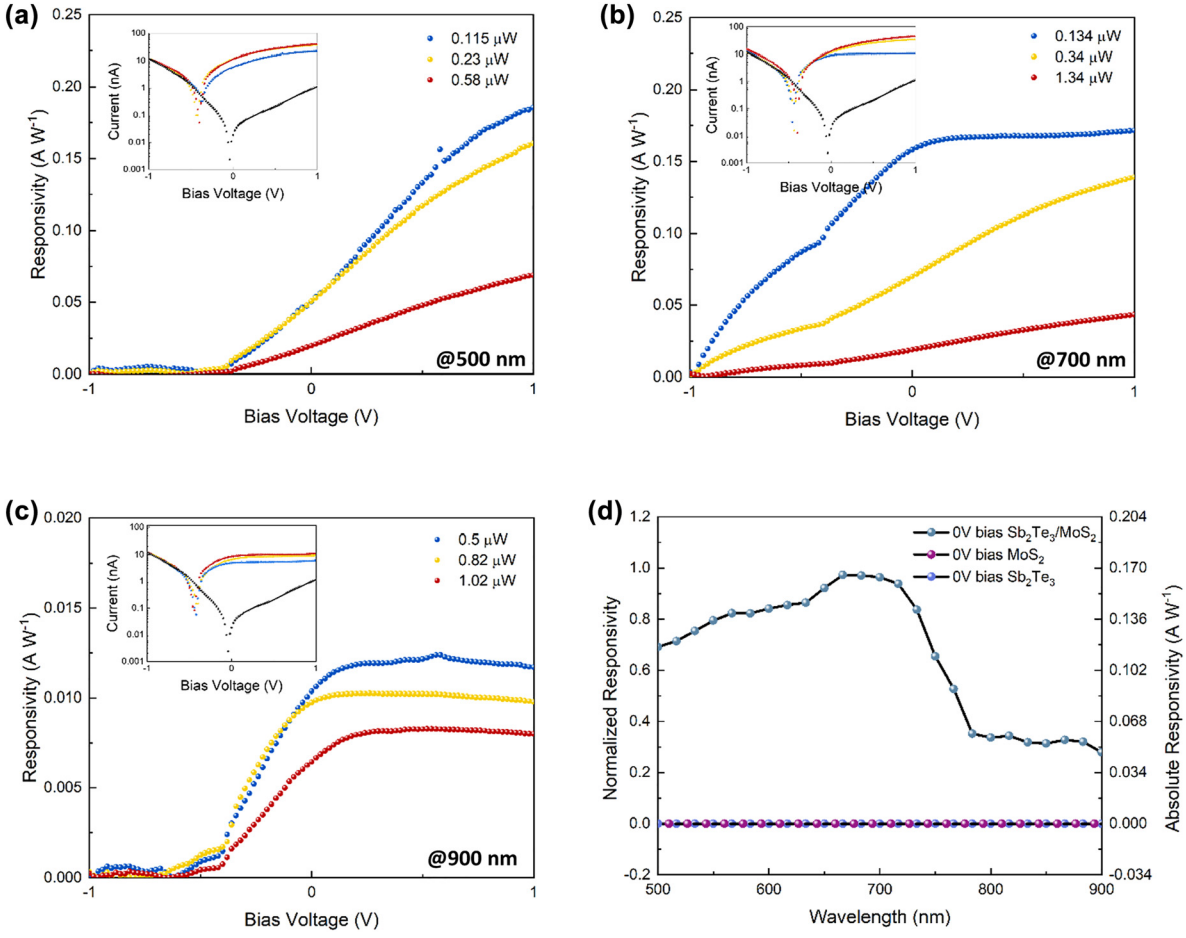

Figure 3: Electrical characterization of Sb_2Te_3/MoS_2 PN junction heterostructure photodetector. (a), (b), (c) The measured photoresponsivity at different wavelengths, 500 nm, 700 nm, and 900 nm, under −1 to 1 V bias voltage. At zero bias, the photoresponsivity was clearly observed and increased proportionally to the optical power. (d) Normalized responsivity by sweeping the wavelength under 0 bias from 500 to 900 nm with a step size of 10 nm, which indicates a broad wavelength response.

function of the optical power at various wavelengths. The I_{photo} increases.

Proportionally to the illuminated optical power, which gives evidence of the photovoltaic effect in the vdW PN heterojunction. The responsivity of the Sb_2Te_3/MoS_2 PN junction-based heterostructure photodetector is measured from −1 V to +1 V at the wavelength of 500 nm, 700 nm, and 900 nm using the free-space optical setup. With a positive bias voltage, an external electric field is formed at the junction interface, increasing the separation efficiency of the photogenerated carriers and, therefore, the responsivity. At +1 V bias, the responsivity was amplified 1.5 to 3 times depending on the wavelength and optical power. The responsivity grows with the applied voltage and gradually saturates depending on the incident optical power. Under zero bias, the significant broadband photocurrent of the PN junction photodetector was observed within a wavelength range from 500 to 900 nm (Figure 3d). The highest responsivity under zero bias was 170 mA W^{-1} at 66 nm.

3 Conclusions

In conclusion, we proposed and experimentally demonstrated a self-powered, extremely sensitive photodetector based on a novel combination of a topological insulator and TMDs van der Waals PN heterojunction. Due to the current rectifying property of the PN heterojunction, the constructed device exhibits extremely low dark current and high responsivities. Under zero bias, the dark current of the device is 2.4 pA, and the responsivity of 170 mA W^{-1}. By increasing the bias voltage to 1 V, the responsivity was magnified thrice due to the external field amplification. This outstanding performance of the proposed photodetector, with its novel material combination, paves the way for further research and applications based on other TMDs and Tis in optoelectronic applications. The PN heterojunction transfer can be easily integrated into waveguide systems, allowing for future applications in PICs.

4 Methods

4.1 Device fabrication

The Sb_2Te_3/MoS_2 PN junction heterostructure is formed using 2D flakes exfoliated from the bulk crystals and transferred by the pick and drop transfer system on Si/SiO_2 substrate. The electrical contact pads were formed using e-beam lithography (Raith Pioneer EBL), and electron beam evaporation was employed to deposit the Ti/Au (5 nm/50 nm) electrodes on the produced heterostructures. The lift-off was performed by acetone, then rinsing in isopropyl alcohol and nitrogen drying in RT (room temperature).

4.2 Device experimentation

The tunable (NKT SUPERCONTINUUM Compact) source and the source meter (Keithly 2600B) were used for electrical response measurements of Sb_2Te_3/MoS_2 PN junction heterostructure devices. The laser beam was focused on the devices by an objective lens. The Raman was performed using a 532 nm laser source at room temperature.

Acknowledgments: This work was performed in part at the George Washington University Nanofabrication and Imaging Center (GWNIC). We thank Professor S. Solares and his student Mr. M. McCraw from the George Washington University for sharing their resources for AFM measurements.

Author contributions: All the authors have accepted responsibility for the entire content of this submitted manuscript and approved submission.

Research funding: This study was funded by AFOSR (FA9550-21-1-0425).

Conflict of interest statement: The authors declare no conflicts of interest regarding this article.

References

[1] Y. Xue, Y Zhang, Y Liu, et al., "Scalable production of a Few-Layer MoS_2/WS_2 vertical heterojunction array and its application for photodetectors," *ACS Nano*, vol. 10, pp. 573−580, 2016.

[2] Y. Huang, F. Zhuge, J. Hou, et al., "Van der Waals coupled organic molecules with monolayer MoS_2 for fast response photodetectors with gate-tunable responsivity," *ACS Nano*, vol. 12, pp. 4062−4073, 2018.

[3] Y. Q. Bie, G. Grosso, M. Heuck, et al., "A $MoTe_2$-based light-emitting diode and photodetector for silicon photonic integrated circuits," *Nat. Nanotechnol.*, vol. 12, pp. 1124−1129, 2017.

[4] R. Cheng, D. Li, H. Zhou, et al., "Electroluminescence and photocurrent generation from atomically sharp WSe_2/MoS_2 heterojunction p-n diodes," *Nano Lett.*, vol. 14, pp. 5590−5597, 2014.

[5] O. Lopez-Sanchez, E. Alarcon Llad, V. Koman, A. Fontcuberta, I. Morral, A. Radenovic, and A. Kis, "Light generation and harvesting in a van der waals heterostructure," *ACS Nano*, vol. 8, pp. 3042−3048, 2014.

[6] W. Zhang, M. H. Chiu, C. H. Chen, W. Chen, L. J. Li, and A. T. S. Wee, "Role of metal contacts in high-performance phototransistors based on WSe2 monolayers," *ACS Nano*, vol. 8, pp. 8653−8661, 2014.

[7] H. Huang, J. Wang, W. Hu, et al., "Highly sensitive visible to infrared $MoTe_2$ photodetectors enhanced by the photogating effect," *Nanotechnology*, vol. 27, pp. 1−7, 2016.

[8] J. Ning, J. C. Martinez, J. Momand, et al., "Differences in Sb_2Te_3 growth by pulsed laser and sputter deposition," *Acta Mater.*, vol. 200, pp. 811–820, 2020.
[9] R. A. Ganeev, V. S. Popov, A. I. Zvyagin, et al., "Exfoliated Bi_2Te_3 nanoparticle suspensions and films: morphological and nonlinear optical characterization," *Nanophotonics*, vol. 10, pp. 3857–3870, 2021.
[10] Q. Yin, G. Si, J. Li, et al., "Self-powered topological insulator Bi_2Te_3/Ge heterojunction photodetector driven by long-lived excitons transfer," *Nanotechnology*, vol. 33, p. 255502, 2022.
[11] S. Ruan, X. Lin, H. Chen, et al., "Terahertz probe of nonequilibrium carrier dynamics and ultrafast photocurrents in the topological insulator Sb_2Te_3," *Appl. Phys. Lett.*, vol. 118, p. 011102, 2021.
[12] M. Z. Hasan and C. L. Kane, "Colloquium: topological insulators," *Rev. Mod. Phys.*, vol. 82, pp. 3045–3067, 2010.
[13] Y.L. Chen, J. G. Analytis, J.-H. Chu, et al., "Experimental Realization of a Three-Dimensional Topological Insulator, Bi_2Te_3," *Science*, vol. 325, no. 5937, pp. 178–181, 2009.
[14] L. Fu, C. L. Kane, and E. J. Mele, "Topological insulators in three dimensions," *Phys. Rev. Lett.*, vol. 98, pp. 1–4, 2007.
[15] S. Z. Butler, S. M. Hollen, L. Cao, et al., "Progress, challenges, and opportunities in two-dimensional materials beyond graphene," *ACS Nano*, vol. 7, pp. 2898–2926, 2013.
[16] H. Zhang, C.-X. Liu, X.-L. Qi, X. Dai, Z. Fang, and S.-C. Zhang, "Topological insulators in Bi_2Se_3, Bi_2Te_3 and Sb_2Te_3 with a single Dirac cone on the surface," *Nat. Phys.*, vol. 5, pp. 438–442, 2009.
[17] I. A. Rahman and A. Purqon, "First principles study of molybdenum disulfide electronic structure," *J. Phys. Conf. Ser.*, vol. 877, p. 012026, 2017.
[18] W. Zhang, J. K. Huang, C. H. Chen, Y. H. Chang, Y. J. Cheng, and L. J. Li, "High-gain phototransistors based on a CVD MoS_2 monolayer," *Adv. Mater.*, vol. 25, pp. 3456–3461, 2013.
[19] K. Roy, M. Padmanabhan, S. Goswami, et al., "Graphene-MoS_2 hybrid structures for multifunctional photoresponsive memory devices," *Nat. Nanotechnol.*, vol. 8, pp. 826–830, 2013.
[20] O. Lopez-sanchez, D. Lembke, M. Kayci, A. Radenovic, and A. Kis, "Ultrasensitive photodetectors based on monolayer MoS_2," *Nat. Nanotechnol.*, vol. 8, pp. 497–501, 2013.
[21] M. Tsai, S. Su, J. Chang, et al., "Monolayer MoS_2 heterojunction solar," *ACS Nano*, vol. 8, pp. 8317–8322, 2014.
[22] M. Bernardi, M. Palummo, and J. C. Grossman, "Extraordinary sunlight absorption and one nanometer thick photovoltaics using two-dimensional monolayer materials," *Nano Lett.*, vol. 13, pp. 3664–3670, 2013.
[23] J. Lou, X. Xu, and P. D. Ye, "Black phosphorus monolayer MoS_2 diode," *ACS Nano*, vol. 8, pp. 8292–8299, 2014.
[24] W. Huang, M. Wang, L. Hu, C. Wang, Z. Xie, and H. Zhang, "Recent advances in semiconducting monoelemental Selenium nanostructures for device applications," *Adv. Funct. Mater.*, vol. 30, pp. 1–25, 2020.
[25] W. Huang, J. Zhu, M. Wang, et al., "Emerging mono-elemental bismuth nanostructures: controlled synthesis and their versatile applications," *Adv. Funct. Mater.*, vol. 31, pp. 1–34, 2021.
[26] W. Huang, L. Hu, Y. Tang, Z. Xie, and H. Zhang, "Recent advances in functional 2D MXene-based nanostructures for next-generation devices," *Adv. Funct. Mater.*, vol. 30, pp. 1–32, 2020.
[27] S. Li, Y. Chen, H. Liu, et al., "Graphdiyne materials as nanotransducer for in vivo photoacoustic imaging and photothermal therapy of tumor," *Chem. Mater.*, vol. 29, pp. 6087–6094, 2017.
[28] M. Wang, J. Zhu, Y. Zi, et al., "Functional two-dimensional black phosphorus nanostructures towards next-generation devices," *J. Mater. Chem. A*, vol. 9, pp. 12433–12473, 2021.
[29] W. Huang, Y. Zhang, Q. You, et al., "Enhanced photodetection properties of tellurium@selenium roll-to-roll nanotube heterojunctions," *Small*, vol. 15, pp. 1–10, 2019.
[30] Y. Zi, J. Zhu, M. Wang, et al., "CdS@CdSe core/shell quantum dots for highly improved self-powered photodetection performance," *Inorg. Chem.*, vol. 60, pp. 18608–18613, 2021.
[31] M. H. Tahersima, Z. Ma, Y. Gui, et al., "Coupling-enhanced dual ITO layer electro-absorption modulator in silicon photonics," *Nanophotonics*, vol. 8, pp. 1559–1566, 2019.
[32] Y. Gui, B. M. Nouri, M. Miscuglio, R. Amin, and H. Wang, "Monolithic ITO Mach – Zehnder interferometer modulator enabling 3500 times higher packing density," *Nanophotonics*, vol. 11, no. 17, pp. 4001–4009, 2022.
[33] R. Amin, J. K. George, H. Wang, et al., "An ITO-graphene heterojunction integrated absorption modulator on Si-photonics for neuromorphic nonlinear activation," *APL Photonics*, vol. 6, no. 12, p. 120801, 2021.
[34] H. Li, J. Wu, Z. Yin, and H. Zhang, "Preparation and applications of mechanically exfoliated single-layer and multilayer MoS_2 and WSe_2 nanosheets," *Acc. Chem. Res.*, vol. 47, pp. 1067–1075, 2014.
[35] H. Li, Q. Zhang, C. C. R. Yap, et al., "From bulk to monolayer MoS_2: evolution of Raman scattering," *Adv. Funct. Mater.*, vol. 22, pp. 1385–1390, 2012.
[36] M. Thripuranthaka, R. V. Kashid, C. Sekhar Rout, and D. J. Late, "Temperature dependent Raman spectroscopy of chemically derived few layer MoS_2 and WS_2 nanosheets," *Appl. Phys. Lett.*, vol. 104, no. 8, p. 081911, 2014.
[37] G. Hao, X. Qi, Y. Fan, et al., "Spiral growth of topological insulator Sb_2Te_3 nanoplates," *Appl. Phys. Lett.*, vol. 102, pp. 1–5, 2013.
[38] G. Zhang, H. Qin, J. Teng, et al., "Quintuple-layer epitaxy of thin films of topological insulator Bi_2Se_3," *Appl. Phys. Lett.*, vol. 95, pp. 95–98, 2009.
[39] K.M.F. Shahil, M. Z. Hossain, V. Goyal, and A. A. Balandin, "Micro-Raman spectroscopy of mechanically exfoliated few-quintuple layers of Bi_2Te_3," *J. Appl. Phys.*, vol. 111, no. 5, p. 054305, 2012.
[40] G. C. Sosso, S. Caravati, and M. Bernasconi, "Vibrational properties of crystalline Sb2Te3 from first principles," *J. Phys. Condens. Matter*, vol. 21, no. 9, p. 095410, 2009.
[41] J. D. Yao, Z. Q. Zheng, J. M. Shao, and G. W. Yang, "Stable, highly-responsive and broadband photodetection based on large-area multilayered WS_2 films grown by pulsed-laser deposition," *Nanoscale*, vol. 7, pp. 14974–14981, 2015.
[42] A. Varghese, D. Saha, K. Thakar, et al., "Near-direct bandgap WSe_2/ReS_2 type-II pn heterojunction for enhanced ultrafast

photodetection and high-performance photovoltaics,'' *Nano Lett.*, vol. 20, pp. 1707–1717, 2020.

[43] Z. Q. Fan, X. W. Jiang, J. Chen, and J. W. Luo, ''Improving performances of in-plane transition-metal dichalcogenide Schottky barrier field-effect transistors,'' *ACS Appl. Mater. Interfaces*, vol. 10, pp. 19271–19277, 2018.

[44] J. W. Chen, S. T. Lo, S. C. Ho, et al., ''A gate-free monolayer WSe_2 pn diode,'' *Nat. Commun.*, vol. 9, no. 1, p. 3143, 2018.

[45] J. Xiao, Y. Zhang, H. Chen, N. Xu, and S. Deng, ''Enhanced performance of a monolayer MoS2/WSe2 heterojunction as a photoelectrochemical cathode,'' *Nano-Micro Lett.*, vol. 10, no. 4, p. 60, 2018.

[46] L. Wang, J. Jie, Z. Shao, et al., ''MoS2/Si heterojunction with vertically standing layered structure for ultrafast, high-detectivity, self-driven visible-near infrared photodetectors,'' *Adv. Funct. Mater.*, vol. 25, pp. 2910–2919, 2015.

[47] R. Tian, X. Gan, C. Li, et al., ''Chip-integrated van der Waals PN heterojunction photodetector with low dark current and high responsivity,'' *Light Sci. Appl.*, vol. 11, no. 1, p. 101, 2022.

[48] M. Dai, H. Chen, F. Wang, et al., ''Ultrafast and sensitive self-powered photodetector featuring self-limited depletion region and fully depleted channel with van der Waals contacts,'' *ACS Nano*, vol. 14, pp. 9098–9106, 2020.

[49] N. Huo, J. Kang, Z. Wei, S. S. Li, J. Li, and S. H. Wei, ''Novel and enhanced optoelectronic performances of multilayer MoS_2 – WS_2 heterostructure transistors,'' *Adv. Funct. Mater.*, vol. 24, pp. 7025–7031, 2014.